SuperDARN observations of high-*m* ULF waves with curved phase fronts and their interpretation in terms of transverse resonator theory

T. K. Yeoman,[1] M. James,[1] P. N. Mager,[2] and D. Y. Klimushkin[2]

Received 28 February 2012; revised 24 April 2012; accepted 18 May 2012; published 29 June 2012.

[1] The Hankasalmi SuperDARN radar in Finland, while operating in a high spatial and temporal resolution mode, has measured the ionospheric signature of a naturally occurring ULF wave in scatter artificially induced by the Tromsø Heater. The wave had a period of 100 s and exhibited curved phase fronts across the heated volume (about 180 km along a single radar beam). Spatial information provided by the radar has enabled an *m*-number for the wave of about 38 to be determined. It is demonstrated here that the curved phase fronts are a generic feature of nonstationary poloidal waves in a transverse resonator, caused by the common action of the field line curvature, the plasma pressure, and the equilibrium current. Some features of the observed event agree with the resonator in the vicinity of the ring current, where it is proposed that the wave is excited by a moving source in the form of a proton cloud drifting in the magnetosphere in the azimuthal direction.

Citation: Yeoman, T. K., M. James, P. N. Mager, and D. Y. Klimushkin (2012), SuperDARN observations of high-*m* ULF waves with curved phase fronts and their interpretation in terms of transverse resonator theory, *J. Geophys. Res.*, *117*, A06231, doi:10.1029/2012JA017668.

1. Introduction

[2] In the terrestrial magnetosphere, Ultra Low Frequency (ULF) waves in the Pc3–5 frequency band (2–100 mHz) represent Alfvén waves standing between the magnetically conjugate points of the high-conductivity ionosphere (for a recent overview, see *Menk* [2011]). These waves are traditionally categorized as toroidal waves if the polarization of their perturbed magnetic field oscillates in an azimuthal direction, and as poloidal waves if the magnetic field oscillates in a radial (meridional) direction, although in reality elliptical polarization is observed, with either the toroidal or poloidal component being dominant. These two kinds of waves generally have a distinct difference in their azimuthal wave number, *m*. The predominantly toroidal modes are generally low-*m* waves (or equivalently have a large scale size in the azimuthal direction) and the predominantly poloidal modes are high-*m* waves (with a correspondingly small scale size in the azimuthal direction).

[3] The two wave modes are also characterized by different radar signatures and are thought to have distinct generation mechanisms. The low-*m* waves are usually considered to be resonantly generated by an incoming fast mode arriving from the outer boundary of the magnetosphere (a field line resonance) [e.g., *Southwood*, 1974]. Observed with radars, these waves show a poleward phase propagation, which may be explained in terms of field line resonance theory [*Walker et al.*, 1979]: the average Alfvén speed normally decreases with latitude, and hence the resonant frequency decreases as well, resulting in a poleward phase propagation.

[4] The high-*m* waves generally have $m > 15$, and are thought to have their energy source in drifting energetic particle fluxes via a kinetic instability caused by non-Maxwellian ion distribution functions, often termed "bump-on-tail" distributions. It is usually supposed that their generation mechanism is through drift or drift-bounce resonance wave-particle interactions [e.g., *Southwood*, 1976; *Karpman et al.*, 1977; *Hughes et al.*, 1979; *Glassmeier et al.*, 1999; *Mager and Klimushkin*, 2005; *Baddeley et al.*, 2005a, 2005b].

[5] Due to the screening action of the atmosphere, the high-*m* waves are only in exceptional cases observed on the ground, and mainly studied by satellites [*Constantinescu et al.*, 2009; *Grimald et al.*, 2009; *Liu et al.*, 2011] and radars [*Fenrich and Samson*, 1997; *Yeoman et al.*, 2006]. As observed with radars, they often exhibit equatorward phase propagation [*Waldock et al.*, 1983; *Tian et al.*, 1991; *Grant et al.*, 1992; *Fenrich et al.*, 1995; *Yeoman et al.*, 1992, 2000]. A possible explanation of the equatorward phase propagation has been suggested by *Mager et al.* [2009]. They suggested that the high-*m* waves are generated by an alternating current associated with substorm-injected proton clouds drifting in the magnetosphere in the azimuthal direction, according to the theory developed earlier in *Mager and Klimushkin* [2007, 2008] and *Zolotukhina et al.* [2008]. If the drift velocity grows with

[1]Department of Physics and Astronomy, University of Leicester, Leicester, UK.
[2]Institute of Solar-Terrestrial Physics, Siberian Branch, Russian Academy of Sciences, Irkutsk, Russia.

Corresponding author: T. K. Yeoman, Department of Physics and Astronomy, University of Leicester, Leicester LE1 7RH, UK. (tim.yeoman@ion.le.ac.uk)

©2012. American Geophysical Union. All Rights Reserved.
0148-0227/12/2012JA017668

the radial coordinate, the particle cloud is stretched into a spiral in the equatorial plane leading to an inward phase motion or, when projected onto the ionosphere, to an equatorward phase propagation. The generation by such a moving source does not contradict the usual instability theory since the moving source can provide an oscillation seed which subsequently will be amplified by means of the instability.

[6] *Yeoman et al.* [2010] identified a new population of ULF wave events, where an equatorward propagating wave characterized by an intermediate azimuthal wave number ($m \approx 13$) was associated with a newly injected moving particle cloud of energetic particles, as elaborated by *Mager and Klimushkin* [2008], *Mager et al.* [2009], and *Zolotukhina et al.* [2008], with, in that case an electron cloud of energy ~33 keV being proposed as the wave source. Earlier, *Pilipenko et al.* [2001] were able to select analogous intermediate-*m* waves in ground data. They explained them as a result of non-resonant generation by transverse non-steady current, which agrees with the interpretation of *Yeoman et al.* [2010].

[7] Here these ideas are elaborated, and a generation mechanism is proposed for a class of events which exhibit uniquely curved phase fronts in latitude. These events were first observed by *Wright and Yeoman* [1999a, 1999b] in the velocities within backscatter induced in the SuperDARN radars using a high power radio frequency transmitter, or ionospheric heater, during a series of experiments, SP-UK-OUCH, performed with the EISCAT heater.

[8] The curved phase fronts imply that the waves are characterized by neither simple poleward nor equatorward phase propagation, thus cannot be explained by the theories outlined above. The previous treatment of the ULF waves' phase motion was based on the assumption of a monotonic dependence of the Alfvénic eigenfrequency on the L-shell. However, regions exist in the magnetosphere (for example the plasmapause and ring current regions) where the Alfvén poloidal eigenfrequency reaches its extremal values [*Vetoulis and Chen*, 1994; *Leonovich and Mazur*, 1995; *Klimushkin*, 1998; *Denton and Vetoulis*, 1998; *Klimushkin et al.*, 2004]. In these regions, transverse resonators or azimuthal waveguides for poloidal Alfvén waves can be formed, where the wave energy is trapped between the conjugate ionospheres and two cut-off magnetic shells, then being channeled along the azimuthal direction [*Vetoulis and Chen*, 1994; *Leonovich and Mazur*, 1995; *Klimushkin*, 1998; *Denton and Vetoulis*, 1998; *Klimushkin et al.*, 2004]. These resonator modes have a discrete spectrum determined by the field line curvature, the plasma pressure, and the equilibrium current.

[9] Previous work has provided only some indirect evidence for the transverse resonators. Several authors [*Denton et al.*, 2003; *Klimushkin et al.*, 2004; *Schäfer et al.*, 2007, 2008] identified poloidal Pc4-5 ULF-waves narrowly localized across magnetic shells with these modes. *Klimushkin et al.* [2004] suggested that the variety of ULF waves known as giant pulsations (Pg) [e.g., *Takahashi et al.*, 2011] are resonator modes on the outer edge of the plasmapause. However, it was not clear whether the spatiotemporal structure of these waves coincide with that predicted by the theory. This study shows that curved phase fronts can be an indicator of the transverse resonators, if the resonator modes are generated by means of some non-stationary processes, including a moving source.

2. Instrumentation

[10] The ionospheric convection velocities presented in this paper were measured by the Hankasalmi SuperDARN radar. SuperDARN is a network of frequency-agile HF coherent scatter radars [*Greenwald et al.*, 1995; *Chisham et al.*, 2007]. A detailed description of the HF radar mode of operation for the interval under study here is given by *Yeoman et al.* [1997]. In the SP-UK-OUCH mode, the Finland radar sounded on only 10 of its 15 beams (0–9), dwelling on each for 1 s, with a range cell length of 15 km, the first range gate being sampled at a range of 480 km. In this study only data from beam 5 of the Finland radar will be illustrated as this beam overlays Tromsø, the location of the EISCAT Heater. The reduced field of view, with beam 5 highlighted in blue, is shown in Figure 1. The EISCAT high-power HF facility or Heater is located at Ramfjordmoen, in the vicinity of Tromsø, Norway. It consists of 12 transmitters feeding a 6 by 6 array (the so-called *array* 2, which was employed during SP-UK-OUCH) of crossed dipole antennas which can be phased to transmit O-, X- or linear mode signals on frequencies in the range 3.9–5.6 MHz. The Heater is capable of radiating over 1 MW of continuous wave power. Further technical details of the Heating facility are given by *Rietveld et al.* [1993]. During this experiment only half of the transmitters were utilized, each having an output of 75 kW. This had two-fold benefits: a reduction in the Heater power consumption, which is acceptable since significant backscatter powers are detected by HF radars for less than full Heater powers [*Wright et al.*, 2006], and the heater beam width was increased (since each transmitter drives a row of six dipole antennas), which generated a larger patch of HF radar backscatter scatter. The transmitted Heater frequency was 4.54 MHz.

3. Data

[11] A run of SP-UK-OUCH was performed on 15 October 1998, from 1200 to 1623 UT, allowing a region of continuous high power backscatter to be generated in the Hankasalmi radar data at 1600 magnetic local time. Data from this experiment, both from the Hankasalmi and the Þykkvibær SuperDARN radars has previously been analyzed in *Wright and Yeoman* [1999a, 1999b].

[12] They noted that the observed ULF wave had a frequency of 11 mHz (91 s period). The Heater generated scatter was observed in several adjacent beams in the Hankasalmi radar. The spatial separation of these measurements enabled the calculation of the effective azimuthal wave number, *m*, of the wave which was found to be 38 ± 6, with westward phase propagation. This corresponds to an east–west wavelength of approximately 360 km at an F-region altitude of 200 km. Combination of data from the Hankasalmi and Þykkvibær SuperDARN radars revealed the wave velocities to have a close to linear polarization in the north-south direction (an east-west polarization in the electric field). Such a polarization ellipse resembles those measured during "Storm-time" Pc5s observed with the STARE VHF radar [e.g., *Allan et al.*,

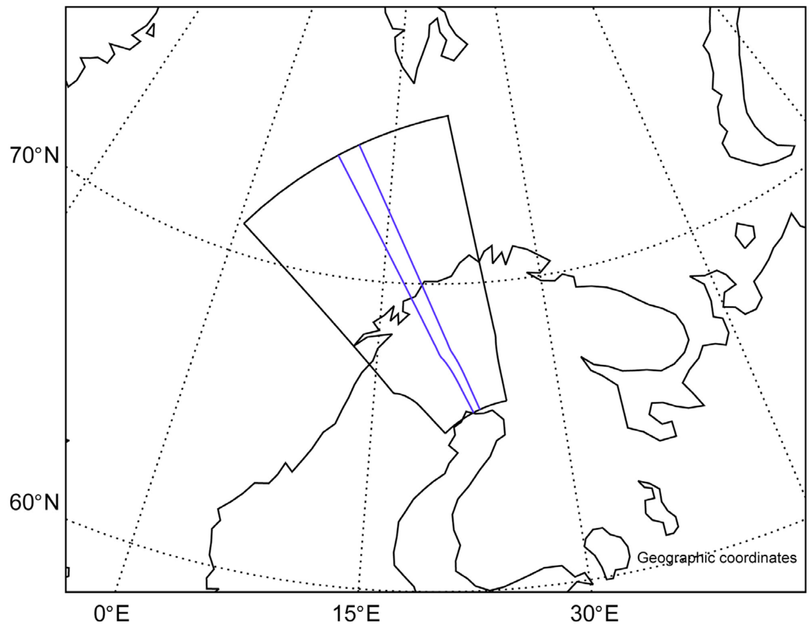

Figure 1. The field of view of the SuperDARN Hankasalmi radar during the SP-UK-OUCH experiments, with beam 5 (which overlies the Tromsø heater) highlighted in blue.

1982]. *Wright and Yeoman* [1999a, 1999b] also highlighted the existence of curved phase fronts in the high-*m* wave observed in the Hankasalmi radar data across a meridional cross-section through the heated volume. Figure 2 presents a detail of a section of the ULF wave which highlights this curvature of the phase fronts. Color-coded line-of-sight velocity data for beam 5 of the radar are presented, where positive velocities represent flow toward the radar. The region of artificial backscatter can clearly be observed between range gates 25 and 36, and the curved phase fronts are particularly clear between 1327–1340 UT. The curvature of the phase fronts suggests a latitudinal scale length of the wave which is of the order of the width of the heated volume (∼180 km). Although the existence of the curiously curved phase fronts was highlighted in *Wright and Yeoman* [1999a, 1999b], no explanation of the phenomenon was offered. The attenuation

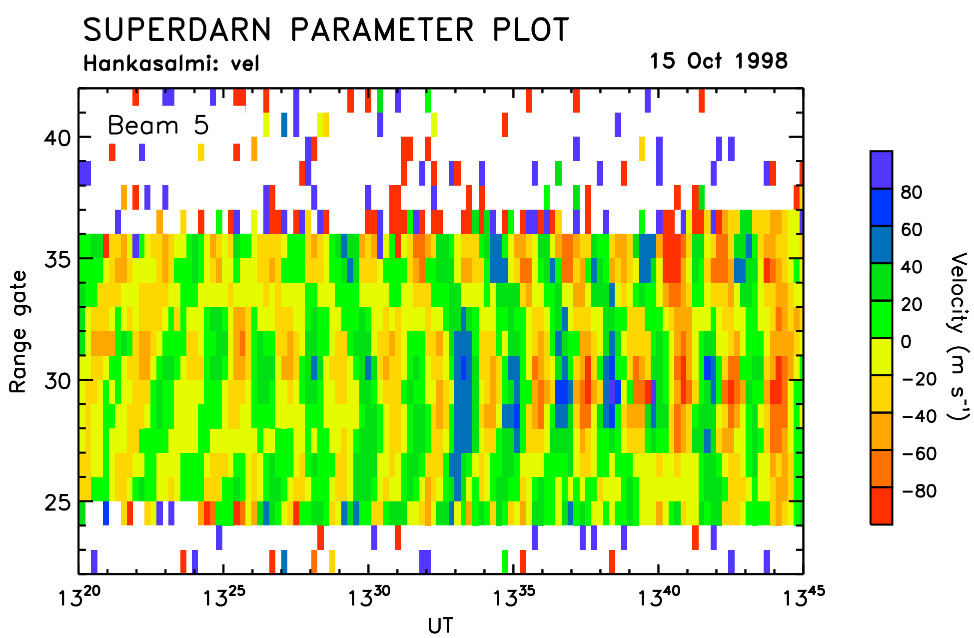

Figure 2. Color-coded line-of-sight velocity from beam 5 of the Hankasalmi SuperDARN radar from 1320 UT–1345 UT on 15 October 1998 as a function of radar range gate and time, illustrating the ULF wave's curved phase fronts.

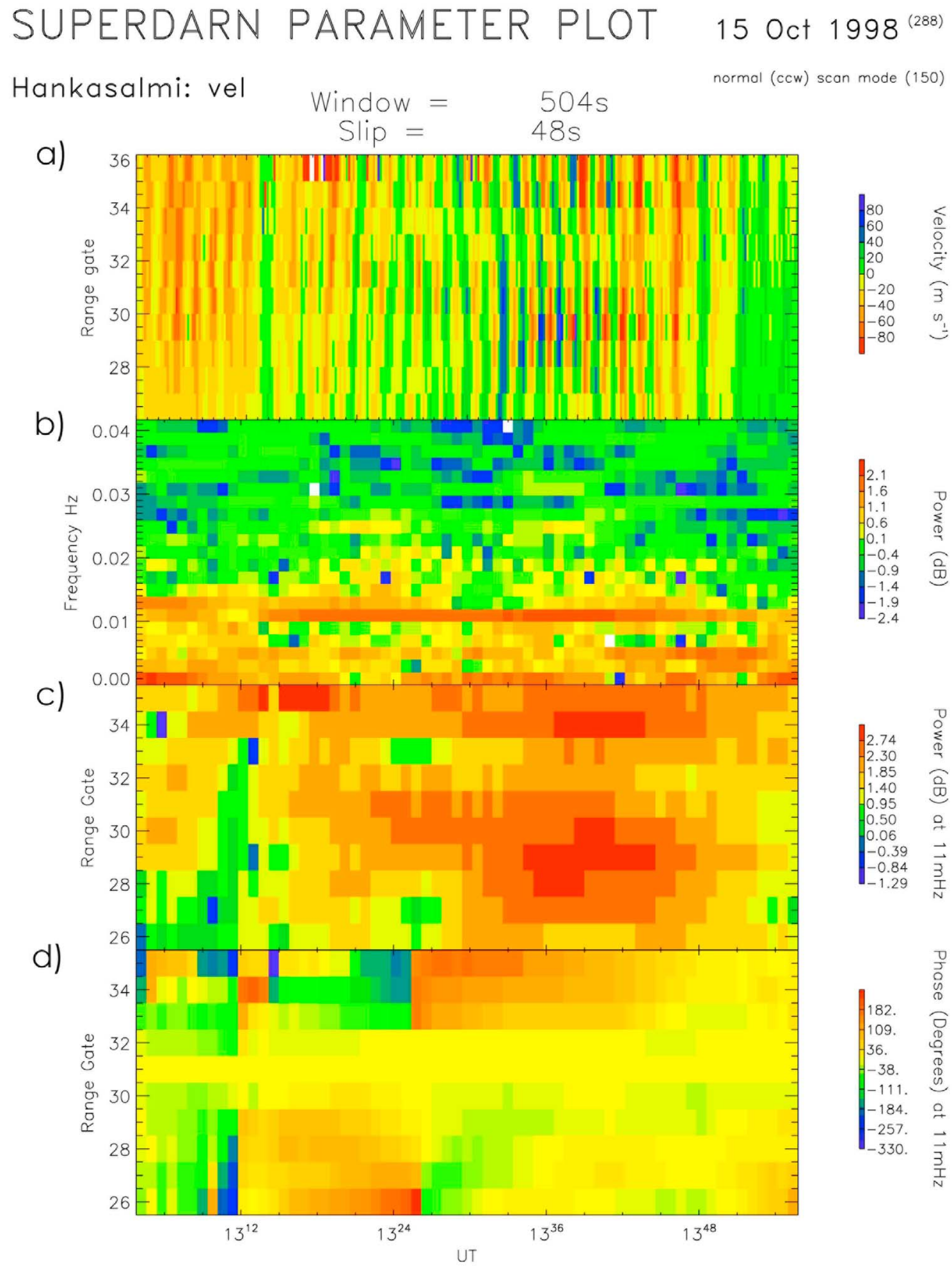

Figure 3. (a) Color-coded line-of-sight velocity from beam 5 of the Hankasalmi SuperDARN radar from 1303 UT–1357 UT on 15 October 1998 as a function of radar range gate and time. (b) A dynamic spectrum of the data in Figure 3a from range gate 31. (c) The Fourier spectral power at a frequency of 10 mHz as a function of radar range gate and time. (d) The Fourier spectral phase, relative to range gate 31, at a frequency of 11 mHz as a function of radar range gate and time.

of the pulsation magnetic perturbation below the ionosphere is proportional to e^{-kz} [e.g., *Hughes and Southwood*, 1976] where k is the field-perpendicular component of the wave number and z is the E-region height. Thus, applying this in the longitudinal and latitudinal directions for the observed wave, the wave attenuation factor is calculated to be approximately 20. Such an attenuation suggests that the wave would not be observed in ground magnetometer data, and indeed it is not [*Wright and Yeoman*, 1999a, 1999b].

[13] Simultaneously with the high-m wave observed on the Hankasalmi radar, however, a low-m field line resonance was observed in ground magnetometer and the Þykkvibær radar data, characterized by a more elliptical polarization ellipse, a frequency of 3.8 mHz (260s) and m = 3–4. The Þykkvibær radar pointed in an east-west direction and so this beam is expected to see strong azimuthal velocities associated with such a global toroidal oscillation of magnetospheric field lines.

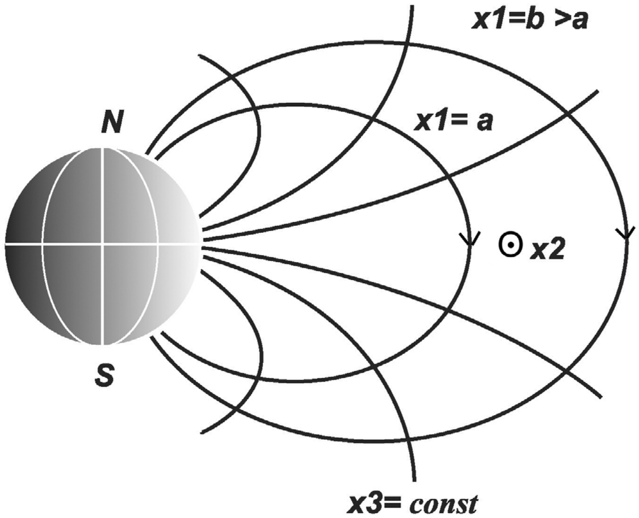

Figure 4. The coordinate system.

[14] Figure 3 displays a longer section of data from the Hankasalmi radar during the experiment, in order to evaluate the characteristics and evolution of the wave phase fronts. Figure 3a again shows color-coded line-of-sight velocity data for beam 5 of the radar, but now for the interval 1303–1357 UT. All the backscatter shown has been artificially generated by the Tromsø Heater, whose ground range from the radar locates it in the center of the band (approximately at range gate 31). This remarkably continuous and uniform band has a spatial extent along the beam of about 12 range gates (180 km). The mean backscatter power during the interval exceeded 30 dB and the data also exhibited very narrow spectral widths which were typically less than 20 m s^{-1}. The data shown were recorded at radar sounding frequencies in the range 19.4–19.7 MHz. The line-of-sight flows observed by the Hankasalmi radar were modulated by a ULF wave signature which appears as a series of bands or stripes during this interval. These measurements represent a data set with an unprecedented spatial, temporal and velocity resolution for HF radar observations of a ULF wave.

[15] Figure 3b shows a dynamic Fourier spectrum of the velocities observed by the Hankasalmi radar in beam 5 at range 31. While the basic time resolution of the data was 10 s, there were occasional brief 1 s interruptions to the time series at the end of radar scans, so the data has been resampled at a constant 12 s for Fourier analysis. The dynamic spectrum uses a window of 504 s with a slip of 48 s. A clear and steady spectral peak at 11 mHz is seen in Figure 3b. The spatial and temporal variation of Fourier spectral power at 11 mHz is explored in Figure 3c. This frequency can be seen to be present over the full extent of radar range included in the plot, and across most of the time interval under study, with the power occurring most strongly between 1315 UT–1354 UT.

[16] Finally Figure 3d presents the Fourier spectral phase, relative to range gate 31, at a frequency of 11 mHz as a function of radar range gate and time. Early in the interval there is little phase variation across the range gates (<50°), and this corresponds to an interval of near-vertical phase fronts in Figure 3a. By 1315 UT the phase fronts have evolved, and a poleward phase propagation can be seen in Figures 3a and 3d, with a total phase change across the latitudinal range of the radar backscatter of ~230°. At 1326 there is a change in this phase behavior, and an equatorward phase propagation of ~250° is observed. Subsequently, from 1330 UT onwards the curved phase fronts become apparent, with a phase lead (relative to range gate 31) of ~100° at the poleward edge of the data and ~30° at the equatorward edge of the data. These curved phase fronts are most clearly seen in Figure 2, and also in Figure 3a centered at 1331–1336 UT.

[17] Such phase behavior is unusual in ULF waves. As outlined in Section 1, waves with low *m* numbers present a poleward phase propagation easily explained in terms of the field line resonance theory [*Walker et al.*, 1979]. High-*m* waves usually exhibit equatorward phase propagation which can be explained by the theory of wave generation by an azimuthally moving source *Mager et al.* [2009]. Neither of those theories explain the curved phase fronts as observed during the event under study. However, both theoretical explanations are based on the assumption of a monotonic dependence of the Alfvénic eigenfrequency on the L-shell. It will be shown below that waves in the regions where the eigenfrequency reaches its extremal value, i.e. where there is a non-monotonic dependence of the Alfvénic eigenfrequency on the L-shell, can exhibit phase behaviors which resemble those observed on October 15, 1998.

4. Theoretical Treatment

4.1. Main Equations

[18] Let us introduce a curvilinear coordinate system $\{x^1, x^2, x^3\}$, in which the field lines have the role of the coordinate lines x^3, i.e. they are lines along which the other two coordinates are invariable (recall that the superscripts and subscripts denote contravariant and covariant coordinates, respectively). In this coordinate system the streamlines are the coordinate lines x^2, and the surfaces of constant pressure (magnetic shells) are the coordinate surfaces $x^1 = const$ (Figure 4). The coordinates x^1 and x^2 have the role of the radial and azimuthal coordinates, and to represent them we shall use the McIlwain parameter L and the azimuthal angle φ, respectively. It is convenient to choose a direction of the azimuthal coordinate coinciding with the proton drift direction. In order for the coordinate system to remain right-handed, the x^3 axis must be directed opposite to the ambient magnetic field. The physical length along a field line is expressed in terms of an increase of the corresponding coordinate as $dl_3 = \sqrt{g_3}dx^3$, where g_3 is the component of the metric tensor, and $\sqrt{g_3}$ is the Lamé coefficient. Similarly, $dl_1 = \sqrt{g_1}dx^1$, and $dl_2 = \sqrt{g_2}dx^2$. The determinant of the metric tensor is $g = g_1g_2g_3$. The equilibrium values of the magnetic field and plasma density are designated as B and ρ. The source of the oscillations is a nonstationary external (azimuthal) current $\vec{j}_{ext}$, formed by drifting substorm injected particles.

[19] An inhomogeneous differential equation which describes Alfvén oscillations generated by a moving source is

$$\mathcal{L}_A\Phi = Q(x^1, x^2, t) \tag{1}$$

[*Mager and Klimushkin*, 2008]. Here $Q(x^1, x^2, t)$ is a source term, and

$$\mathcal{L}_A = \frac{\partial}{\partial x^1}\left[-\frac{\sqrt{g}}{g_1}\frac{1}{A^2}\frac{\partial^2}{\partial t^2}+\frac{\partial}{\partial x^3}\frac{g_2}{\sqrt{g}}\frac{\partial}{\partial x^3}\right]\frac{\partial}{\partial x^1} + \frac{\partial}{\partial x^2}\left[-\frac{\sqrt{g}}{g_2}\frac{1}{A^2}\frac{\partial^2}{\partial t^2}+\frac{\sqrt{g}}{g_2}\eta+\frac{\partial}{\partial x^3}\frac{g_1}{\sqrt{g}}\frac{\partial}{\partial x^3}\right]\frac{\partial}{\partial x^2}$$

is the Alfvén differential operator, where $A = B/\sqrt{4\pi\rho}$ is the Alfvén speed, Φ is a scalar function ("potential"). The electric field of the Alfvén mode can be represented in the form

$$\vec{E} = -\nabla_\perp \Phi \tag{2}$$

since the parallel electric field is absent due to infinite plasma conductivity ($\nabla_\perp$ is the transverse gradient operator). Here η is usually called the ballooning term,

$$\eta = -\frac{2}{R}\left(\frac{4\pi}{c}\frac{J}{B}+\frac{2}{R}\frac{s^2}{A^2}\right), \tag{3}$$

R^{-1} is the field line local curvature, J is the stationary current and s is the sound velocity [e.g., *Denton*, 1998; *Klimushkin et al.*, 2004].

[20] The boundary conditions are chosen as

$$\Phi\Big|_{x^1,x^2\to\pm\infty} = 0, \qquad \Phi\Big|_{x^3_\pm} = 0. \tag{4}$$

Here the second condition corresponds to the full wave reflection from the ionosphere ($x^3_\pm$ denotes the points of the intersection of the field line with the ionosphere).

[21] If the source term is the external current in the magnetosphere, then it can be represented as

$$Q(x^1, x^2, t) = -\frac{4\pi}{c^2}\sqrt{g}\frac{\partial}{\partial x^2}\frac{\partial}{\partial t}j^2_{ext}, \tag{5}$$

where $j^2_{ext} = j_{ext}/\sqrt{g_2}$ is the contra-variant azimuthal projection of the vector $\vec{j}_{ext}$.

[22] In order to solve the wave equation (1), we perform the Fourier-transform of this equation over φ and t. As a result, we obtain a differential equation only with respect to two variables, x^1 and x^3:

$$\hat{L}_A \Phi_{m\omega} = \tilde{q}_{m\omega}, \tag{6}$$

where ω and m are the parameters of the Fourier transform over time (frequency) and azimuthal angle (azimuthal wave number), $\tilde{q}_{m\omega}$ is the Fourier-image of $Q(x, \varphi, t)$, and $\hat{L}_A$ is the Fourier-image of the Alfvénic operator $\mathcal{L}_A$ analogous to the Alfvénic operator for the monochromatic wave with frequency ω and azimuthal wave number m, defined as

$$\hat{L}_A \equiv \frac{\partial}{\partial x^1}\hat{L}_T(\omega)\frac{\partial}{\partial x^1} - m^2\hat{L}_P(\omega), \tag{7}$$

where

$$\hat{L}_T(\omega) = \frac{\partial}{\partial x^3}\frac{g_2}{\sqrt{g}}\frac{\partial}{\partial x^3}+\frac{\sqrt{g}}{g_1}\frac{\omega^2}{A^2} \tag{8}$$

is the toroidal mode operator, and

$$\hat{L}_P(\omega) = \frac{\partial}{\partial x^3}\frac{g_1}{\sqrt{g}}\frac{\partial}{\partial x^3}+\frac{\sqrt{g}}{g_2}\left(\frac{\omega^2}{A^2}+\eta\right), \tag{9}$$

is the poloidal mode operator. The eigenvalues of these operators with the boundary condition on the ionosphere (equation (4)) are denoted Ω_{TN} and Ω_{PN}, respectively (here N is the parallel harmonic number). They are called the toroidal and poloidal eigenfrequencies since they characterize the purely azimuthal (toroidal) and radial (poloidal) oscillations of field lines [e.g., *Leonovich and Mazur*, 1997; *Klimushkin et al.*, 2004].

[23] The method for the solution of equation (6) has been developed by *Klimushkin et al.* [2004]. As was shown there, the function $\Phi_{m\omega}$ can be represented as

$$\Phi_{m\omega} \approx R_N(x^1)T_N(x^1, x^3), \tag{10}$$

where $T_N(x^1, x^3)$ is an eigenfunction of the toroidal operator $\hat{L}_T$, defining a longitudinal structure of the N-th harmonic standing between ionospheres. The normalization condition is

$$\left\langle \frac{\sqrt{g}}{g_1}\frac{T_N^2}{A^2}\right\rangle = 1, \tag{11}$$

(here the angle brackets designate integration along the field line between the ionospheres, $\langle..\rangle = \int_{x^3_-}^{x^3_+}(..)dx^3$). The function $R_N(x^1)$ describes the structure of this harmonic across the magnetic shells.

[24] Further, if we substitute the function $\Phi_{m\omega}(x^1, x^3)$ from equation (10) into equation (6), we obtain the ordinary differential equation defining the radial structure of the wavefield:

$$\frac{\partial}{\partial x^1}(\omega^2 - \Omega^2_{TN}(x^1))\frac{\partial}{\partial x^1}R_N - \frac{m^2}{L^2}(\omega^2 - \Omega^2_{PN}(x^1))R_N = q(x^1, \omega, m). \tag{12}$$

Here $q(x^1, \omega, m) = \langle \tilde{q}_{m\omega} T_N\rangle$ (see *Klimushkin et al.* [2004] and *Leonovich and Mazur* [1997] for more detail).

4.2. The Transverse Resonators

[25] In a magnetosphere characterized by curved field lines, the Alfvénic eigenfrequency depends on the direction of the field line oscillations: the poloidal oscillations (with a large radial component of the wave's magnetic field and a large azimuthal component of the electric field) and the toroidal oscillations (conversely with a large azimuthal component of the magnetic field and a large radial component of the electric field) have different eigenfrequencies [e.g., *Leonovich and Mazur*, 1997]. As is seen from equations (8) and (9) the poloidal eigenfrequency is also significantly influenced by the finite plasma pressure and equilibrium current. While the toroidal eigenfrequency in the WKB approximation on the parallel coordinate is given by the usual Alfvén dispersion relation, $\Omega^2_{TN} = k^2_\parallel A^2$,

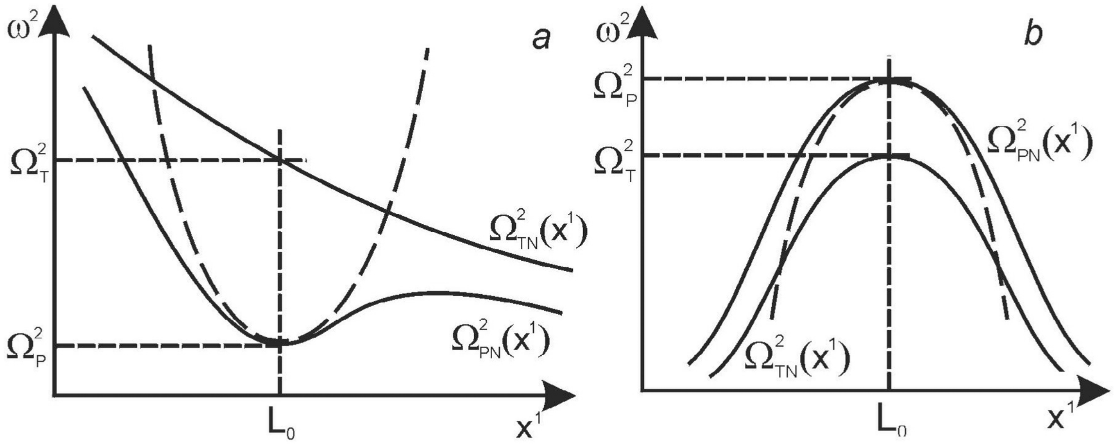

Figure 5. The dependence of the toroidal Ω_{TN} and poloidal Ω_{PN} frequencies on the radial coordinate x^1 in the region of the transverse resonator (a) near the ring current and (b) on the plasmapause.

the poloidal mode in a curved magnetic field with finite-β plasma has the dispersion relation

$$\Omega_{PN}^2 = (k_{\|}^2 - \eta)A^2,$$

where the ballooning term η was determined in equation (3) above. This dispersion relation can be obtained both in MHD and (under some approximations) in kinetics [*Klimushkin and Mager*, 2011].

[26] Special regions of the magnetosphere (the plasmapause and ring current) may be characterized by extremal values of the poloidal eigenfrequency Ω_{PN} as a function of the radial coordinate x^1, as illustrated in Figure 5. Near the plasmapause, both functions $\Omega_{TN}(x^1)$ and $\Omega_{PN}(x^1)$ reach their maximal values due to large density gradients. In the region of the ring current, the function $\Omega_{PN}(x^1)$ has a minimum due to the plasma pressure P inward gradient (westward equilibrium current in the magnetosphere). With a very strong ring current, it is even possible that $\Omega_{PN}^2 < 0$, that is, the system is unstable due to the ballooning instability [e.g., *Liu*, 1997; *Agapitov et al.*, 2008]. Although ballooning-stable plasma configurations are more typical, the westward current causes a dip in the poloidal eigenfrequency [*Denton and Vetoulis*, 1998; *Klimushkin et al.*, 2004].

[27] In both plasmapause and ring current regions, a transverse resonator can be formed, where the Alfvén mode is trapped across the magnetic surfaces between some cut-off shells [*Vetoulis and Chen*, 1994; *Leonovich and Mazur*, 1995; *Klimushkin*, 1998; *Denton and Vetoulis*, 1998]. Let us consider these regions in more detail.

4.3. The Structure of a Single Fourier Harmonic in the Transverse Resonator

[28] For the sake of simplicity, in the regions where the poloidal eigenfrequency $\Omega_{PN}(x^1)$ has extreme values, we can avail ourselves of the expansion

$$\Omega_{PN}^2(x^1) = \Omega_P^2\left[1 \pm \left(\frac{x^1 - L_0}{l}\right)^2\right], \tag{13}$$

where the "+" sign refers to the case where the resonator is localized near the minimum of the function $\Omega_{PN}(x^1)$, and the "−" sign refers to the maximum of $\Omega_{PN}(x^1)$, Ω_P and L_0 are the value of the extrema of $\Omega_{PN}(x^1)$ and its position, respectively. Further, we can neglect the toroidal frequency variation across the resonator:

$$\Omega_{TN}(x^1) = const = \Omega_T, \tag{14}$$

where $\Omega_T = \Omega_{TN}(L_0)$.

[29] In the case of the minimum (the "+" sign in equation (13)), equation (12) can be reduced to the form

$$\frac{\partial^2}{\partial \xi^2}R + (\sigma - \xi^2)R = -q\frac{L_0 l}{m\Omega_P}(\Omega_T^2 - \omega^2)^{-1/2}. \tag{15}$$

Here

$$\xi = \left(\frac{m\Omega_P}{L_0 l}\right)^{1/2}(\Omega_T^2 - \omega^2)^{-1/4}x,$$

where $x = x^1 - L_0$,

$$\sigma = \frac{ml}{L_0\Omega_P}\cdot\frac{\omega^2 - \Omega_P^2}{(\Omega_T^2 - \omega^2)^{1/2}}. \tag{16}$$

If the right hand part of equation (15) is zero, this equation is of the same form as the Schrödinger equation for a harmonic oscillator. As is well known, the solution to this equation is bounded outside of the region of mode localization, requiring that the parameter σ be quantized, $\sigma = 2n + 1$, where $n =$ 0, 1, 2,.. is an integer. From this we have the wave frequency quantization condition:

$$\omega_n^2 = \Omega_P^2 + \Delta\omega_n^2, \tag{17}$$

where

$$\Delta\omega_n^2 = -\frac{1}{2}\left(\frac{L_0\Omega_P}{ml}\right)^2(2n+1)^2 + \frac{1}{2}\sqrt{\left(\frac{L_0\Omega_P}{ml}\right)^4(2n+1)^4 + 4\Delta\Omega^2\left(\frac{L_0\Omega_P}{ml}\right)^2(2n+1)^2},$$

$$\Delta\Omega^2 = \Omega_T^2 - \Omega_P^2.$$

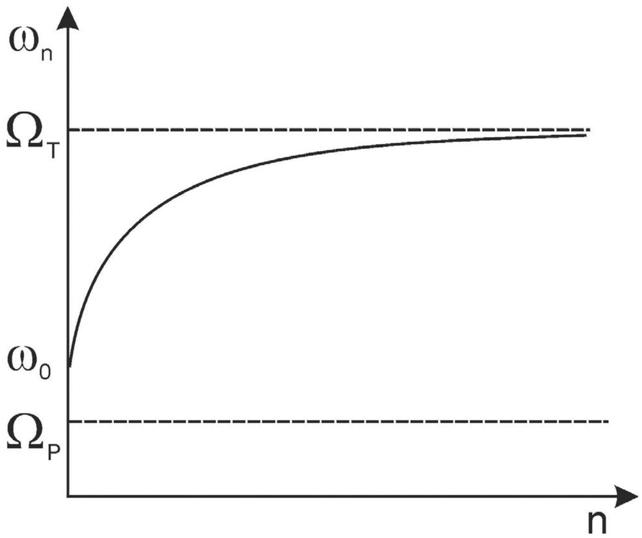

Figure 6. The dependence of the wave frequency on harmonic number n in the region of the resonator near the ring current (a minimum in $\Omega_{PN}(x^1)$).

From equation (17) it then follows that the wave frequency is limited by Ω_T and Ω_P as shown in Figure 6.

[30] The solution of equation (15) satisfying the boundary conditions (4) is

$$R_N(x,\omega,m) = -\sum_{n=0}^{\infty} \frac{C_n}{(\sigma-\sigma_n)(\Omega_T^2-\omega^2)^{1/2}} R_n. \qquad (18)$$

Here

$$C_n = \frac{L_0 l}{m\Omega_P} \int_{-\infty}^{+\infty} qR_n d\xi, \qquad (19)$$

$$R_n = \pi^{-1/4} 2^{-n/2} (n!)^{-1/2} H_n(\xi) e^{-\xi^2/2}, \qquad (20)$$

where H_n are Hermite polynomials.

4.4. The Structure and Evolution of the Nonstationary Wavefield

[31] In the following, we are going to consider the spatiotemporal structure of the resonator modes excited by two different kinds of non-stationary sources: an impulsive source and a moving source comprised of drifting substorm-injected particles. In both cases, the wave equation (1) can be solved by means of the reverse Fourier transform of the solution (6):

$$\Phi(x^1,x^2,x^3,t) = \int_{-\infty}^{+\infty} d\omega \int_{-\infty}^{+\infty} dm\, \Phi_{m\omega} e^{im\varphi - i\omega t}. \qquad (21)$$

Thus, according to equations (21) and (10), the solution of the wave equation (1) is

$$\Phi(x^1,x^2,x^3,t) = \mathcal{R}_N(x^1,x^2,t) T_N(x^1,x^3), \qquad (22)$$

where the function

$$\mathcal{R}_N(x^1,x^2,t) = \int_{-\infty}^{+\infty} d\omega \int_{-\infty}^{+\infty} dm\, R_N(m,\omega) e^{im\varphi - i\omega t} \qquad (23)$$

defines both the transverse structure of the wave and its evolution.

[32] In the following, we will consider only the several significant n-harmonics, which have the frequencies close to Ω_P. Thus, the expression for R_N (18) can be reduced to the approximate form

$$R_N(x,\omega,m) \approx -\frac{L_0\Omega_P}{ml} \sum_{n=0}^{\infty} \frac{C_n}{(\omega^2-\omega_n^2)} R_n \qquad (24)$$

4.4.1. The Case of an Impulse Source

[33] Following *Mager and Klimushkin* [2006], let us consider an impulse source given by

$$j^2_{ext} = j_0\, \delta(t) e^{im_0\varphi}.$$

Thus, in equation (12) for this kind of source

$$q(x^1,\omega,m) = q_0 m_0 \omega \delta(m-m_0),$$
$$q_0 = -\frac{2}{c^2}\left\langle j_0 \sqrt{g} T_N \right\rangle.$$

In this case, in equation (24)

$$C_n = \frac{L_0 l}{m\Omega_P} q_0 m_0 \omega \delta(m-m_0)\, \tilde{C}_n,$$

where

$$\tilde{C}_n = \begin{cases} 0, \text{when } n = 2j+1, (j=0,1\ldots), \\ \pi^{-1/4} 2^{-j} \sqrt{(2j)!} (j!)^{-1} \sqrt{2\pi}, \text{when } n = 2j. \end{cases}$$

Then from equations (23) and (24) we finally obtain the solution for the case of a resonator localized near a minimum of the function $\Omega_{PN}(x^1)$,

$$\mathcal{R}_N \approx -2\pi i q_0 \frac{L_0^2}{m_0} \sum_{n=0}^{\infty} \tilde{C}_n \tilde{R}_n(x) \cos(\omega_n t) e^{im\varphi}. \qquad (25)$$

Here

$$\tilde{R}_n(x) = R_n(\xi = \xi_n),$$

where

$$\xi_n = \left(\frac{m_0\Omega_P}{L_0 l}\right)^{1/2} (\Omega_T^2 - \omega_n^2)^{-1/4} x.$$

The solution for the case where the resonator is localized near the maximum of the function $\Omega_{PN}(x^1)$ is similar to equation (25) but it has sign "+" and other expressions for quantities ω_n and ξ_n:

$$\omega_n^2 = \Omega_P^2 - \Delta\omega_n^2,$$
$$\Delta\Omega^2 = \Omega_P^2 - \Omega_T^2,$$

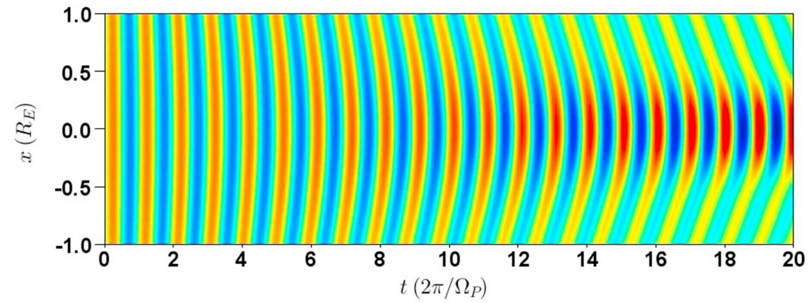

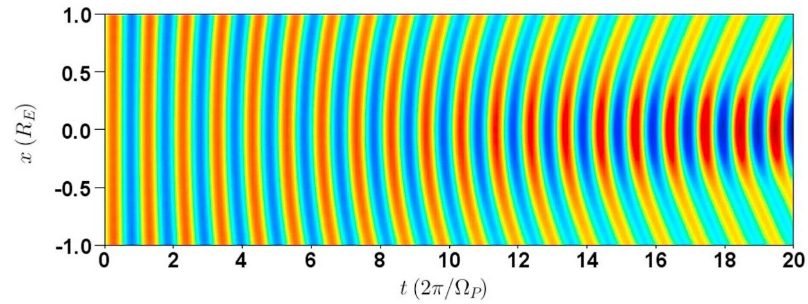

Figure 7. The azimuthal component of the electric field as a function of radial coordinate and time for the impulse source model. (top) The case near a minimum of the function $\Omega_{PN}(x^1)$ and (bottom) that near a maximum of the function $\Omega_{PN}(x^1)$.

and

$$\xi_n = \left(\frac{m_0\Omega_P}{L_0 l}\right)^{1/2}(\omega_n^2 - \Omega_T^2)^{-1/4}x.$$

[34] Figure 7 shows the temporal evolution of the radial structure of the azimuthal electric field of the impulse excited wave for locations near both minima and maxima in $\Omega_{PN}(x^1)$.

4.4.2. The Case of a Moving Source

[35] The cloud of drifting particles comprising the external current (shown schematically in Figure 8) is assumed to be narrowly localized in azimuth, that is the contra-variant azimuthal projection of the external current

$$j^2_{ext} = en_0\,\omega_d\,\delta(\varphi - \omega_d t)\Theta(t), \tag{26}$$

where $\omega_d(x^1)$ is the bounce-averaged angular drift velocity, e and n_0 are the electric charge and number density of the particles, and φ is the azimuthal angle, which can be used as the x^2 coordinate. The physical component of the current can be obtained by using the linear drift velocity $V = \sqrt{g_2}\omega_d$ instead of the angular velocity in equation (26). Thus, for this kind of source in equation (12)

$$\begin{aligned} q(x^1, \omega, m) &= q_0 m\omega\delta(\omega - m\omega_d), \\ q_0 &= -2\frac{e\omega_d}{c^2}\left\langle n_0\sqrt{g}T_N\right\rangle. \end{aligned} \tag{27}$$

[36] Let us consider the case when ω_d is independent of x^1. In this case

$$C_n = \frac{L_0 l}{m\Omega_P}q_0 m\omega\delta(\omega - m\omega_d)\tilde{C}_n,$$

where

$$\tilde{C}_n = \begin{cases} 0, \text{when } n = 2j+1, (j = 0, 1\ldots), \\ \pi^{-1/4}2^{-j}\sqrt{(2j)!}(j!)^{-1}\sqrt{2\pi}, \text{when } n = 2j. \end{cases}$$

As result, the expression defining both the transverse structure of the wavefield and its evolution for the case of a

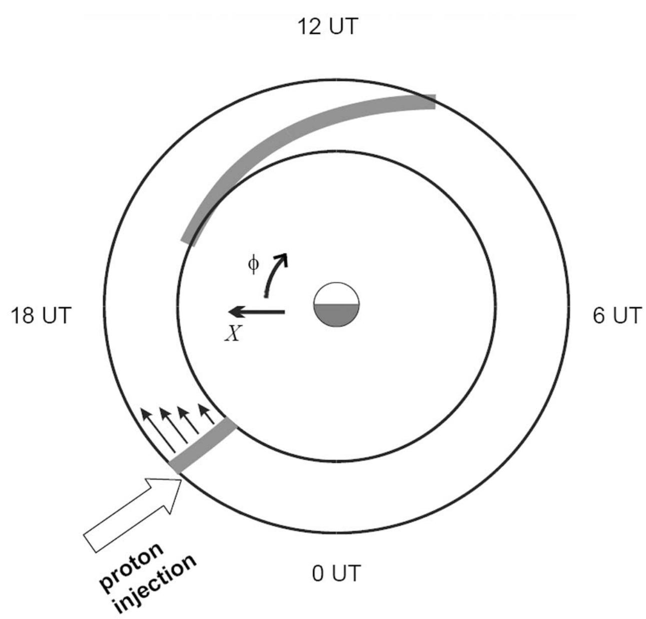

Figure 8. The model of the moving source.

resonator localized near a minimum of the function $\Omega_{PN}(x^1)$ is

$$\mathcal{R}_N(x,\varphi,t) = -q_0 L_0^2 \sum_{n=0}^{\infty} \tilde{C}_n \times \int_{-\infty}^{+\infty} d\omega \int_{-\infty}^{+\infty} dm \frac{\omega R_n \delta(\omega - m\omega_d) e^{im\varphi - i\omega t}}{m(\omega^2 - \omega_n^2)}. \quad (28)$$

[37] First we integrate equation (27) over ω. Since under the integral there is a delta function depending on ω, we obtain

$$\mathcal{R}_N(x,\varphi,t) = -q_0 L_0^2 \omega_d \sum_{n=0}^{\infty} \tilde{C}_n \times \int_{-\infty}^{+\infty} dm \frac{R_n e^{im\varphi - im\omega_d t}}{(m^2\omega_d^2 - \omega_n^2)}. \quad (29)$$

In order to integrate this we use the residue theorem. Poles of the integrated function are given by the expression

$$m^2 = \frac{\omega_n^2(m)}{\omega_d^2}. \quad (30)$$

[38] Solutions of this equation are limited, since ω_n is limited by $\Omega_P < \omega_n < \Omega_T$. Furthermore, the difference between toroidal Ω_T and poloidal Ω_P eigenfrequencies is usually small in the magnetosphere, $\Delta\Omega^2 = \Omega_T^2 - \Omega_P^2 \ll \Omega_T^2, \Omega_P^2$. Under these conditions, we can solve equation (30) approximately: let

$$m^2 = \frac{\Omega_P^2}{\omega_d^2} + \delta m^2,$$

where $\delta m^2 \ll \Omega_P^2/\omega_d^2$, then from (30) and (17) we have

$$\frac{\Omega_P^2}{\omega_d^2} + \delta m^2 = \frac{\Omega_P^2}{\omega_d^2} + \frac{\Delta\omega_n^2(m^2 = \Omega_P^2/\omega_d^2 + \delta m^2)}{\omega_d^2},$$

whence it follows that

$$\delta m^2 \approx \frac{\Delta\omega_n^2(m^2 = \Omega_P^2/\omega_d^2)}{\omega_d^2}.$$

Thus we have two poles $\pm m_n$, where

$$m_n \equiv \frac{\tilde{\omega}_n}{\omega_d},$$

and $\tilde{\omega}_n = \omega_n(m = \Omega_P/\omega_d)$. Finally, we obtain the approximate expression for $\mathcal{R}_N$:

$$\mathcal{R}_N \approx 2\pi q_0 L_0^2 \Theta(\omega_d t - \varphi) \times \sum_{n=0}^{\infty} \frac{\tilde{C}_n}{\tilde{\omega}_n} \tilde{R}_n(x) \sin(\tilde{\omega}_n t - m_n\varphi). \quad (31)$$

In equation (31) the expression $\Theta(\omega_d t - \varphi)$ is due to taking into account the causality principle. Here

$$\tilde{\omega}_n^2 = \Omega_P^2 + \Delta\tilde{\omega}_n^2,$$

where

$$\Delta\tilde{\omega}_n^2 = \frac{1}{2}\omega_d^2 (L_0/l)^2 (2n+1)^2 \times \left[\sqrt{1 + 4(\Delta\Omega^2/\omega_d^2)(l/L_0)^2/(2n+1)^2} - 1\right],$$

$$\Delta\Omega^2 = \Omega_T^2 - \Omega_P^2,$$

and

$$\tilde{R}_n(x) = R_n(\xi = \xi_n),$$

where

$$\xi_n = \left(\frac{m_n \Omega_P}{L_0 l}\right)^{1/2} (\Omega_T^2 - \tilde{\omega}_n^2)^{-1/4} x.$$

The solution for the case where the resonator is localized near the maximum of the function $\Omega_{PN}(x^1)$ is similar to equation (31) but it has sign "$-$" and other expressions for quantities $\tilde{\omega}_n$ and ξ_n:

$$\tilde{\omega}_n^2 = \Omega_P^2 - \Delta\tilde{\omega}_n^2,$$

where

$$\Delta\tilde{\omega}_n^2 = \frac{1}{2}\omega_d^2 (L_0/l)^2 (2n+1)^2 \times \left[\sqrt{1 + 4(\Delta\Omega^2/\omega_d^2)(l/L_0)^2/(2n+1)^2} - 1\right],$$

$$\Delta\Omega^2 = \Omega_P^2 - \Omega_T^2,$$

and

$$\xi_n = \left(\frac{m_n \Omega_P}{L_0 l}\right)^{1/2} (\tilde{\omega}_n^2 - \Omega_T^2)^{-1/4} x.$$

[39] In the case when ω_d is a function of x^1, from equations (23), (24), and (19) it follows that the expression defining both transverse structure of the wavefield and its evolution for the case of a resonator localized near a minimum of the function $\Omega_{PN}(x^1)$ is

$$\mathcal{R}_N(x,\varphi,t) \approx -q_0 L_0^2 \sum_{n=0}^{\infty} \int_{-\infty}^{+\infty} dx' \int_{-\infty}^{+\infty} d\omega \int_{-\infty}^{+\infty} dm \times \left(\frac{m\Omega_P}{L_0 l}\right)^{1/2} (\Omega_T^2 - \omega^2)^{-1/4} \delta(\omega - m\omega_d(x')) \times \frac{\omega R_n(m,\omega,x) R_n(m,\omega,x') e^{im\varphi - i\omega t}}{m(\omega^2 - \omega_n^2)}.$$

Integrating this expression first over ω and then over m (analogously to the integration procedure for the case where ω_d was independent of x^1) we finally have

$$\mathcal{R}_N(x,\varphi,t) \approx 2\pi q_0 L_0^2 \cdot \sum_{n=0}^{\infty} \int_{-\infty}^{+\infty} dx' \left[\frac{m_n(x')\Omega_P}{L_0 l}\right]^{1/2} \frac{[\Omega_T^2 - \tilde{\omega}_n^2(x')]^{-1/4}}{\tilde{\omega}_n(x')} \cdot \tilde{R}_n(x') \tilde{R}_n(x) \sin(\tilde{\omega}_n(x')t - m_n(x')\varphi) \Theta(\omega_d(x')t - \varphi), \quad (32)$$

where

$$\tilde{R}_n(x') \equiv R_n(m = m_n(x'), \omega = \tilde{\omega}_n(x'), x'),$$
$$\tilde{R}_n(x) \equiv R_n(m = m_n(x'), \omega = \tilde{\omega}_n(x'), x),$$
$$\tilde{\omega}_n(x') \equiv \tilde{\omega}_n(\omega_d = \omega_d(x')), m_n(x') = \tilde{\omega}_n(x')/\omega_d(x').$$

[40] Figure 9 shows the wavefield structure determined by the solution (32) at two different time instances (note that azimuth $\varphi = 0$ corresponds to the point where the source begins its azimuthal movement and does not represent a fixed local time of 06:00). Note that the wave is characterized by curved phase fronts for four hours of local time westward of the initial particle injection region. Further westward of this the phase propagation becomes equatorwards. Figure 10 shows the evolution of the radial structure over time at a fixed azimuthal location, and again shows a significant interval of wave activity characterized by curved phase fronts.

5. Discussion

[41] As is seen from Figures 7, 9, and 10, the wave packets generated in the transverse resonator by both impulsive and moving sources share the same common feature, curved phase fronts, which can be considered to be a good indicator of the resonator. In the case of a resonator near the ring current (a minimum in the $\Omega_{PN}(x^1)$ function) the phase fronts at the edges of the resonator are ahead of the phase fronts at the center for the resonator. This behavior is due to the superposition of the resonator modes. The eigenfrequencies of the modes are close to each other and increase with increasing harmonic number. At the outset the fundamental harmonic with the lowest frequency dominates at the center and higher harmonics dominate at the edges of the resonator. In case of a resonator on the plasmapause (a maximum in the function $\Omega_{PN}(x^1)$ (see Figure 7, bottom)) the picture is opposite: the phase fronts at the edges of the resonator are behind the phase fronts at the center, since the eigenfrequencies of the modes decrease with increasing harmonic number.

[42] A difference between the impulsive source cases illustrated in Figure 7 and the moving source case illustrated in Figures 9 and 10 is that the phase fronts in the former case are always symmetric with respect to the center of the resonator, and hence no predominant radial phase propagation is observed. In the latter case, however, there must be predominantly equatorward (poleward) phase propagation if the drift velocity grows (decreases) with the radial coordinate. In addition, in the former case the m number is arbitrary, whereas in the latter case it is defined by the ratio of the wave frequency to the drift velocity of the cloud, $m = \omega/\Omega_d$.

[43] A direct comparison can be made between the results of the theoretical study and the data taken on 15 October 1998. As can be seen from Figure 3d, the wave phase changes abruptly at 1310 UT and 1326 UT, thus the waves observed in the intervals before 1310 UT, between 1310 UT and 1326 UT, and after 1326 UT can be considered as separate wave packets. The wave packet in the interval after 1326 UT has the highest power (see Figure 3c) and the clearest structure. This packet will be used for comparison below. As seen from Figures 2 and 3a the phase fronts at the edges of the wave packet are ahead of those at the center. Such a picture corresponds to that which is obtained theoretically for a wave packet in the transverse resonator near the ring current (see Figure 7 for minimum of the function Ω_{PN} and Figure 10). Another feature of this observed wave packet is an overall predominance of equatorward phase propagation. This may be explained by the generation of waves by a drifting cloud of energetic protons with a drift velocity depending on the radial coordinate as shown in Figure 8. As a result of such a generation mechanism we would obtain a wave packet with an equatorward phase propagation, the magnetospheric spatial structure of which is shown in Figure 9 and the temporal evolution at a fixed azimuthal location is shown in Figure 10. A well defined value of the azimuthal wave number, in this case 38 ± 6, is additional evidence for this generation mechanism. In this case, the observed azimuthal wave number corresponds to an energy of $\sim$100 keV for the protons in the cloud.

[44] While for the event presented here there are no conjugate spacecraft available to provide direct observations of the driving particle population, ground-based observations of the magnetic field can provide some context for the observations. Magnetic activity during the event as measured by the Kp index was moderate at 2− to 2+, with no significant enhancement in the Dst index observed. However, at 0800 UT the AL index showed a strong negative deflection to −500 nT, which lasted for 3 hours, subsequently dropping to −300 nT by the time of the wave observations. The magnetometer stations contributing to AL were in the Canadian sector, close to midnight. Thus there is evidence of substorm activity prior to and during the wave event, which presumably provided the westward-drifting energetic proton population. Future studies will hopefully combine ionospheric observations with in situ spacecraft data in order to more quantitatively test transverse resonator theory, with direct measurements of both the Alfvén speed profile and energetic particle populations. The upcoming NASA Radiation Belt Storm Probes mission will provide opportunities for such experiments.

6. Conclusions

[45] A high-m wave event observed on October 15, 1998, exhibits curved phase fronts which cannot be explained by earlier theories, which demanded either poleward or equatorward phase propagation. It is shown here that such phase behavior is typical for poloidal Alfvén waves in the regions of the transverse resonator. The features of the event under study are consistent with a transverse resonator in the vicinity of the ring current, where the poloidal eigenfrequency reaches a minimum value [*Vetoulis and Chen*, 1994; *Klimushkin*, 1998; *Denton and Vetoulis*, 1998].

[46] In addition, some features of the observed high-m wave hint that the wave was generated by a moving source, such as a proton cloud drifting in the magnetosphere in the azimuthal direction. Earlier, the theory of such an Alfvén wave generation mechanism was applied as an explanation for the equatorward phase propagation of high-m waves observed with radars [*Mager et al.*, 2009], and was able to explain a change in the polarization of substorm associated Pc5 pulsations [*Zolotukhina et al.*, 2008]. Future work, combining ionospheric observations of the ULF wavefields and in-situ observations of the drifting plasma populations

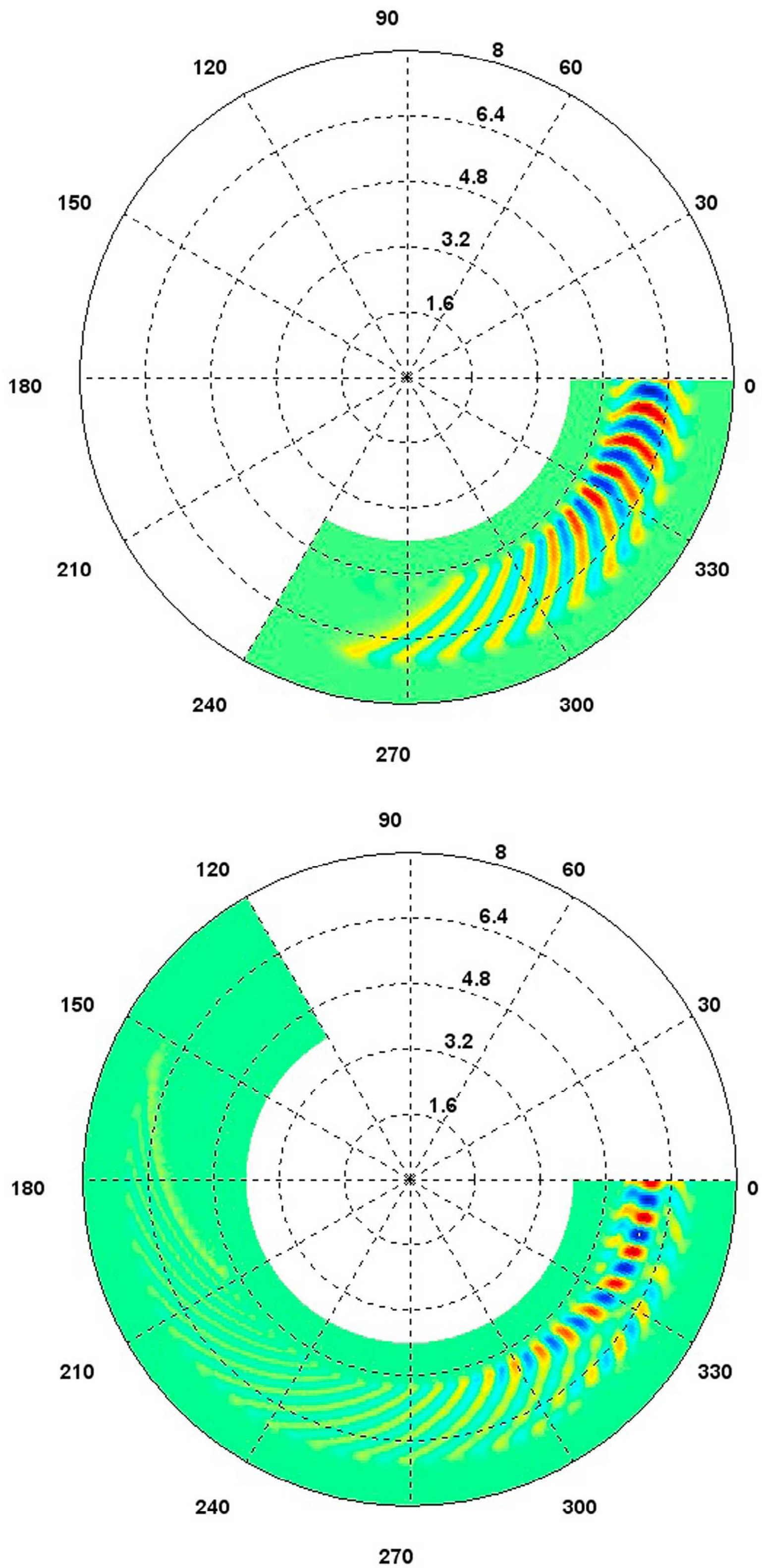

Figure 9. The azimuthal component of the electric field in the equatorial plane at two different time instances, (top) $t_1 = 10(2\pi\Omega_P^{-1})$ and (bottom) $t_2 = 20(2\pi\Omega_P^{-1})$, for the moving source model near a minimum of the function $\Omega_{PN}(x^1)$. Azimuth $\phi = 0$ corresponds to the point where the source begins its azimuthal movement. The radial coordinate corresponds to the distance from the Earth center, in Earth radii.

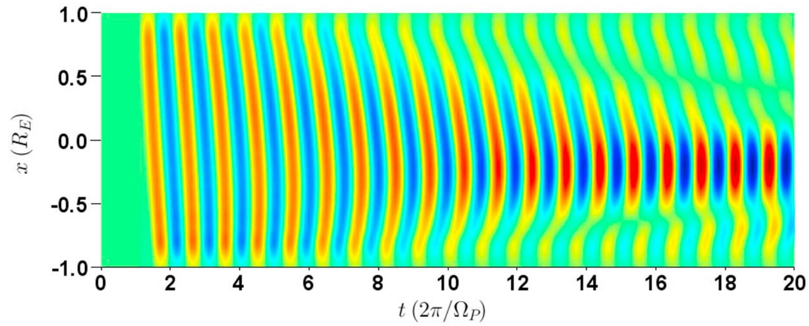

Figure 10. The azimuthal component of the electric field in the equatorial plane for the moving source model near a minimum of the function $\Omega_{PN}(x^1)$, as a function of radial coordinate and time at a fixed azimuthal location.

will be required to elucidate to what extent the observed high-*m* waves are generated by kinetic plasma instabilities, by drifting particle sources, or perhaps by some combination of both mechanisms.

[47] **Acknowledgments.** The work by T.K.Y. is supported by STFC grant ST/H002480/1. M.J. was supported by a NERC studentship. The work by D.K. and P.M. is supported by RFBR grants 12-02-00305-a, 12-05-00121-a, and 12-05-98522-a, Program of the presidium of the Russian Academy of Sciences 22, and OFN RAS 16. The Hankasalmi SuperDARN radar operations were funded by STFC grant PP/E007929/1.

[48] Robert Lysak thanks the reviewers for their assistance in evaluating this paper.

References

Agapitov, A. V., O. K. Cheremnykh, and A. S. Parnowski (2008), Ballooning perturbations in the inner magnetosphere of the Earth: Spectrum, stability and eigenmode analysis, *Adv. Space Res.*, *41*, 1682–1687, doi:10.1016/j.asr.2006.12.040.

Allan, W., E. M. Poulter, and E. Nielsen (1982), STARE observations of a Pc 5 pulsation with large azimuthal wave number, *J. Geophys. Res.*, *87*(A8), 6163–6172, doi:10.1029/JA087iA08p06163.

Baddeley, L. J., T. K. Yeoman, and D. M. Wright (2005a), HF Doppler sounder measurements of the ionospheric signatures of small scale ULF waves, *Ann. Geophys.*, *23*(5), 1807–1820, doi:10.5194/angeo-23-1807-2005.

Baddeley, L. J., T. K. Yeoman, D. M. Wright, K. J. Trattner, and B. J. Kellet (2005b), On the coupling between unstable magnetospheric particle populations and resonant high *m* ULF wave signatures in the ionosphere, *Ann. Geophys.*, *23*(2), 567–577, doi:10.5194/angeo-23-567-2005.

Chisham, G., et al. (2007), A decade of the Super Dual Auroral Radar Network (SuperDARN): Scientific achievements, new techniques and future directions, *Surv. Geophys.*, *28*, 33–109, doi:10.1007/s10712-007-9017-8.

Constantinescu, O. D., et al. (2009), THEMIS observations of duskside compressional Pc5 waves, *J. Geophys. Res.*, *114*, A00C25, doi:10.1029/2008JA013519.

Denton, R. E. (1998), Compressibility of the poloidal mode, *J. Geophys. Res.*, *103*(A3), 4755–4760, doi:10.1029/97JA02652.

Denton, R. E., and G. Vetoulis (1998), Global poloidal mode, *J. Geophys. Res.*, *103*(A4), 6729–6739, doi:10.1029/97JA03594.

Denton, R. E., M. R. Lessard, and L. M. Kistler (2003), Radial localization of magnetospheric guided poloidal Pc4-5 waves, *J. Geophys. Res.*, *108*(A3), 1105, doi:10.1029/2002JA009679.

Fenrich, F. R., and J. C. Samson (1997), Growth and decay of field line resonances, *J. Geophys. Res.*, *102*(A9), 20,031–20,039, doi:10.1029/97JA01376.

Fenrich, F. R., J. C. Samson, G. Sofko, and R. A. Greenwald (1995), ULF high- and low-*m* field line resonances observed with the Super Dual Auroral Radar Network, *J. Geophys. Res.*, *100*(A11), 21,535–21,547, doi:10.1029/95JA02024.

Glassmeier, K.-H., S. Buchert, U. Motschmann, A. Korth, and A. Pedersen (1999), Concerning the generation of geomagnetic giant pulsations by drift-bounce resonance ring current instabilities, *Ann. Geophys.*, *17*(3), 338–350, doi:10.1007/s00585-999-0338-4.

Grant, I. F., D. R. McDiarmid, and A. G. McNamara (1992), A class of high-*m* pulsations and its auroral radar signature, *J. Geophys. Res.*, *97*(A6), 8439–8451, doi:10.1029/92JA00434.

Greenwald, R. A., et al. (1995), DARN/SuperDARN: A global view of the dynamics of high-latitude convection, *Space Sci. Rev.*, *71*, 761–796, doi:10.1007/BF00751350.

Grimald, S., et al. (2009), Modulation of NTC frequencies by Pc5 ULF pulsations: Experimental test of the generation mechanism and magnetoseismology of the emitting surface, *J. Geophys. Res.*, *114*, A11211, doi:10.1029/2009JA014270.

Hughes, W. J., and D. J. Southwood (1976), The screening of micropulsation signals by the atmosphere and ionosphere, *J. Geophys. Res.*, *81*(19), 3234–3240, doi:10.1029/JA081i019p03234.

Hughes, W., R. Mcpherron, J. Barfield, and B. Mauk (1979), A compressional Pc4 pulsation observed by three satellites in geostationary orbit near local midnight, *Planet. Space Sci.*, *27*(6), 821–840, doi:10.1016/0032-0633(79)90010-2.

Karpman, V. I., B. I. Meerson, A. B. Mikhailovsky, and O. A. Pokhotelov (1977), The effects of bounce resonances on wave growth rates in the magnetosphere, *Planet. Space Sci.*, *25*(6), 573–585, doi:10.1016/0032-0633(77)90064-2.

Klimushkin, D. Y. (1998), Resonators for hydromagnetic waves in the magnetosphere, *J. Geophys. Res.*, *103*, 2369–2375, doi:10.1029/97JA02193.

Klimushkin, D. Y., and P. N. Mager (2011), Spatial structure and stability of coupled Alfvén and drift compressional modes in non-uniform magnetosphere: Gyrokinetic treatment, *Planet. Space Sci.*, *59*, 1613–1620, doi:10.1016/j.pss.2011.07.010.

Klimushkin, D. Y., P. N. Mager, and K.-H. Glassmeier (2004), Toroidal and poloidal Alfvén waves with arbitrary azimuthal wave numbers in a finite pressure plasma in the Earth's magnetosphere, *Ann. Geophys.*, *22*, 267–288.

Leonovich, A. S., and V. A. Mazur (1995), Magnetospheric resonator for transverse-small-scale standing Alfvén waves, *Planet. Space Sci.*, *43*, 881–883, doi:10.1016/0032-0633(94)00206-7.

Leonovich, A. S., and V. A. Mazur (1997), A model equation for monochromatic standing Alfvén waves in the axially symmetric magnetosphere, *J. Geophys. Res.*, *102*(A6), 11,443–11,456, doi:10.1029/96JA02523.

Liu, W. W. (1997), Physics of the explosive growth phase: Ballooning instability revisited, *J. Geophys. Res.*, *102*, 4927–4931, doi:10.1029/96JA03561.

Liu, W., et al. (2011), Spatial structure and temporal evolution of a dayside poloidal ULF wave event, *Geophys. Res. Lett.*, *38*, L19104, doi:10.1029/2011GL049476.

Mager, P. N., and D. Y. Klimushkin (2005), Spatial localization and azimuthal wave numbers of Alfvén waves generated by drift-bounce resonance in the magnetosphere, *Ann. Geophys.*, *23*, 3775–3784.

Mager, P. N., and D. Y. Klimushkin (2006), On impulse excitation of the global poloidal modes in the magnetosphere, *Ann. Geophys.*, *24*, 2429–2433, doi:10.5194/angeo-24-2429-2006.

Mager, P. N., and D. Y. Klimushkin (2007), Generation of Alfvén waves by a plasma inhomogeneity moving in the Earth's magnetosphere, *Plasma Phys. Rep.*, *33*, 391–398.

Mager, P. N., and D. Y. Klimushkin (2008), Alfvén ship waves: high-*m* ULF pulsations in the magnetosphere, generated by a moving plasma inhomogeneity, *Ann. Geophys.*, *26*, 1653–1663.

Mager, P. N., D. Y. Klimushkin, and N. Ivchenko (2009), On the equatorward phase propagation of high-*m* ULF pulsations observed by radars, *J. Atmos. Sol. Terr. Phys.*, *71*, 1677–1680, doi:10.1016/j.jastp.2008.09.001.
Menk, F. W. (2011), Magnetospheric ULF waves: A review, in *The Dynamic Magnetosphere*, *IAGA Spec. Sopron Book Ser.*, vol. 3, edited by W. Liu and M. Fujimoto, pp. 223–256, Springer, Dordrecht, Netherlands.
Pilipenko, V., N. Kleimenova, O. Kozyreva, M. Engebretson, and O. Rasmussen (2001), Long-period magnetic activity during the May 15, 1997 storm, *J. Atmos. Sol. Terr. Phys.*, *63*(5), 489–501, doi:10.1016/S1364-6826(00)00189-9.
Rietveld, M. T., H. Kohl, H. Kopka, and P. Stubbe (1993), Introduction to ionospheric heating at Tromsø—I. Experimental overview, *J. Atmos. Sol. Terr. Phys.*, *55*(4–5), 577–599, doi:10.1016/0021-9169(93)90007-L.
Schäfer, S., K. H. Glassmeier, P. T. I. Eriksson, V. Pierrard, K. H. Fornaçon, and L. G. Blomberg (2007), Spatial and temporal characteristics of poloidal waves in the terrestrial plasmasphere: A CLUSTER case study, *Ann. Geophys.*, *25*(4), 1011–1024, doi:10.5194/angeo-25-1011-2007.
Schäfer, S., K. H. Glassmeier, P. T. I. Eriksson, P. N. Mager, V. Pierrard, K. H. Fornaçon, and L. G. Blomberg (2008), Spatio-temporal structure of a poloidal Alfvén wave detected by Cluster adjacent to the dayside plasmapause, *Ann. Geophys.*, *26*(7), 1805–1817, doi:10.5194/angeo-26-1805-2008.
Southwood, D. J. (1974), Some features of field line resonances in the magnetosphere, *Planet Space Sci.*, *22*, 483–491, doi:10.1016/0032-0633(74)90078-6.
Southwood, D. J. (1976), A general approach to low-frequency instability in the ring current plasma, *J. Geophys. Res.*, *81*(19), 3340–3348, doi:10.1029/JA081i019p03340.
Takahashi, K., K.-H. Glassmeier, V. Angelopoulos, J. Bonnell, Y. Nishimura, H. J. Singer, and C. T. Russell (2011), Multisatellite observations of a giant pulsation event, *J. Geophys. Res.*, *116*, A11223, doi:10.1029/2011JA016955.
Tian, M., T. Yeoman, M. Lester, and T. Jones (1991), Statistics of Pc 5 pulsation events observed by SABRE, *Planet. Space Sci.*, *39*(9), 1239–1247, doi:10.1016/0032-0633(91)90037-B.
Vetoulis, G., and L. Chen (1994), Global structures of Alfvén-ballooning modes in magnetospheric plasmas, *Geophys. Res. Lett.*, *21*(19), 2091–2094, doi:10.1029/94GL01703.
Waldock, J., T. Jones, E. Nielsen, and D. Southwood (1983), First results of micropulsation activity observed by SABRE, *Planet. Space Sci.*, *31*(5), 573–578, doi:10.1016/0032-0633(83)90046-6.
Walker, A. D. M., R. A. Greenwald, W. F. Stuart, and C. A. Green (1979), STARE auroral radar observations of Pc 5 geomagnetic pulsations, *J. Geophys. Res.*, *84*(A7), 3373–3388, doi:10.1029/JA084iA07p03373.
Wright, D. M., and T. K. Yeoman (1999a), CUTLASS observations of a high-*m* ULF wave and its consequences for the DOPE HF Doppler sounder, *Ann. Geophys.*, *17*(11), 1493–1497, doi:10.1007/s00585-999-1493-3.
Wright, D. M., and T. K. Yeoman (1999b), High resolution bistatic HF radar observations of ULF waves in artificially generated backscatter, *Geophys. Res. Lett.*, *26*(18), 2825–2828, doi:10.1029/1999GL900606.
Wright, D. M., J. A. Davies, T. K. Yeoman, T. R. Robinson, and H. Shergill (2006), Saturation and hysteresis effects in ionospheric modification experiments observed by the CUTLASS and EISCAT radars, *Ann. Geophys.*, *24*, 543–553, doi:10.5194/angeo-24-543-2006.
Yeoman, T., M. Tian, M. Lester, and T. Jones (1992), A study of Pc5 hydromagnetic waves with equatorward phase propagation, *Planet. Space Sci.*, *40*(6), 797–810, doi:10.1016/0032-0633(92)90108-Z.
Yeoman, T. K., D. M. Wright, T. R. Robinson, J. A. Davies, and M. T. Rietveld (1997), High spatial and temporal resolution observations of an impulse-driven field line resonance in radar backscatter artificially generated with the Tromsø heater, *Ann. Geophys.*, *15*, 634–644, doi:10.1007/s00585-997-0634-9.
Yeoman, T. K., D. M. Wright, P. J. Chapman, and A. B. Stockton-Chalk (2000), High-latitude observations of ULF waves with large azimuthal wavenumbers, *J. Geophys. Res.*, *105*(A3), 5453–5462, doi:10.1029/1999JA005081.
Yeoman, T. K., D. M. Wright, and L. J. Baddeley (2006), Ionospheric signatures of ULF waves: Active radar techniques, in *Magnetospheric ULF Waves: Synthesis and New Directions*, *Geophys. Monogr. Ser.*, vol. 169, edited by K. Takahashi et al., pp. 273–288, AGU, Washington, D. C.
Yeoman, T. K., D. Y. Klimushkin, and P. N. Mager (2010), Intermediate-*m* ULF waves generated by substorm injection: A case study, *Ann. Geophys.*, *28*, 1499–1509, doi:10.5194/angeo-28-1499-2010.
Zolotukhina, N. A., P. N. Mager, and D. Y. Klimushkin (2008), Pc5 waves generated by substorm injection: A case study, *Ann. Geophys.*, *26*(7), 2053–2059, doi:10.5194/angeo-26-2053-2008.